Description and stability analysis of nonlinear transmission line type metamaterials using nonlinear dynamics theory

Sameh Y. Elnaggar and Gregory N. Milford

Citation: Journal of Applied Physics **121**, 124902 (2017); doi: 10.1063/1.4979022
View online: http://dx.doi.org/10.1063/1.4979022
View Table of Contents: http://aip.scitation.org/toc/jap/121/12
Published by the American Institute of Physics

Description and stability analysis of nonlinear transmission line type metamaterials using nonlinear dynamics theory

Sameh Y. Elnaggar[a] and Gregory N. Milford[b]
School of Engineering and Information Technology, University of New South Wales, Canberra, Australian Capital Territory 2600, Australia

(Received 16 December 2016; accepted 10 March 2017; published online 24 March 2017)

Nonlinear metamaterials offer a potential technology to realize applications at microwave, terahertz, and optical frequencies. However, due to the strong and controlled nonlinearity, the wave interactions can be quite complex. In the current article, a framework based on nonlinear dynamics theory is developed to describe such complex interactions. This is demonstrated for the case of a harmonically pumped nonlinear left handed transmission line through the use of bifurcation theory, stability analysis, and linearization about the limit cycle to calculate the autonomously generated frequencies and their spatial distributions. Higher order parametric interactions, which can be mediated by the strong nonlinearity, are automatically included in the model. It is demonstrated that autonomous components can be visualized in both the phase and the set of solution spaces. The framework is general in terms of the transmission line configuration, the nature and strength of the nonlinearity, and the number of stages. It also provides accurate results when the autonomous frequencies are in the vicinity of the Bragg frequency. *Published by AIP Publishing*.
[http://dx.doi.org/10.1063/1.4979022]

I. INTRODUCTION

Metamaterials are artificial materials that exhibit properties not found in nature, such as negative refractive indexes and the propagation of left and right-handed waves.[1,2] Left-handed or Composite Right-Left handed transmission lines (CRLH TLs) were proposed as a platform to realize metamaterials.[3,4] Due to the distributed nature of TL based structures, CRLH TLs exhibit wider bandwidths and lower losses compared with resonance based systems. The possibility of controlling the left and right-handed propagation properties in such structures introduced a paradigm shift that has been successfully applied to the design and realization of novel devices in the microwave regime.[3–7]

Nonlinear (NL) optics is that branch of optics which exploits the nonlinear properties of natural materials, with applications such as second, third, and higher harmonic generation and optical parametric amplification.[8] The nonlinearity is usually due to the nonlinear response of the dielectric polarization to the applied electric field. *Nonlinear metamaterials* were introduced as a merge between the two fields: Metamaterials and Nonlinear Optics.[9–12] Due to the strong and controlled nonlinearity, the realm of nonlinear metamaterials opens the door for new potential applications using the novel and intriguing properties predicted by nonlinear metamaterials, such as backward phase matching—the so-called nonlinear mirror.[13] Additionally, the impossibility of shock wave formation makes it possible to exploit parametric interactions to design low noise parametric amplifiers,[14] particularly in frequency ranges where active devices are not available or are impractical such as in the mm-wave and terahertz frequency bands.

Various experiments with nonlinear (NL) CRLH TLs have reported a range of interesting phenomena, such as harmonic, subharmonic, and parametric generation,[14,15] envelope solitons,[16] and multistabilty.[17] However, the presence of strong nonlinearities makes the analysis of NL CRLH TL systems quite challenging. For example, for varactor loaded NL CRLH TLs not only can the fundamental (pump) wave generate parametric frequencies, but also the relatively strong higher harmonics can couple with the strong nonlinearity to generate parametric components.[16] Another challenge is the excitation of multiple pairs of autonomous frequencies,[18] making *wave mixing* approaches impractical due to the need to identify a number of unknown frequencies a priori. Moreover, it was experimentally and numerically observed that the autonomous frequencies might be close to the lowest Bragg frequency.[19] In this case, the wavelengths of the spontaneously generated autonomous frequencies are comparable to the unit cell length; hence, the *effective homogeneity condition* is violated and the TL behaves more like a photonic crystal.[4] Based on quasi-phase matching arguments, it was shown that the biasing network can play a role in material polling in optics,[8] which in turn has a profound effect on the values of the autonomous frequencies. However, unlike multi-wavelength sized periodic poled crystals in nonlinear optical media, the nonlinearity introduced here is contained within a unit cell and hence microscopic (sub-wavelength) in nature.[20]

In this article, we establish a general framework based on nonlinear dynamics (NLD) theory to rigorously investigate the properties of NL CRLH TL structures. This is implemented using a nonlinear state space model (SSM) formulation that describes the time dependent interactions between the various states in the system[21,22]

$$\dot{\mathbf{x}}(t) = f(\mathbf{x}(t), \mathbf{u}(t)), \tag{1}$$

[a]Electronic mail: s.elnaggar@unsw.edu.au
[b]Electronic mail: g.milford@adfa.edu.au

where $\mathbf{x}$ and $\mathbf{u}$ are the time varying state and excitation vectors, respectively, f is some nonlinear operator, and $\dot{\mathbf{x}}(t)$ indicates the time derivative of $\mathbf{x}(t)$ with respect to time t. Such a form automatically invites the application of rigorous, multi-disciplinary NLD theory.[21,23] Nonlinear dynamics is robust, allows the nonlinearity to be arbitrary, and is valid for 1D, 2D, and 3D structures. The NLD based approach is applicable to both short and long TLs, since it automatically includes complex effects due to strong nonlinearity and/or pump, and can be regarded as an *ab-initio* approach that is directly related to the physics of the system. For almost all the practical cases, the TL is truncated and matched to the connected load and source. However in the presence of a strong pump, the line characteristic impedance can be non-uniform and time varying. Hence, reflections from both the source and the load might strongly affect the system behaviour. Moreover, spatial periodicity is irrelevant to the state space formulation since only locally applied circuit relationships (Ohm's and Kirchoff's laws) are required to formulate (1). Using NLD, particularly stability and bifurcation theories, it was demonstrated that the excitation of the autonomous frequencies, in the presence of a strong pump, is equivalent to a bifurcation from a limit cycle to a torus in the phase space.[24] Due to the generality of the NLD approach, this conclusion is valid for all the NL CRLH lines, regardless of their length, nature of nonlinearity, pump strength, circuit configuration, and dimension. For infinitely long transmission lines, the number of state variables will be infinite and the analysis automatically reduces to the coupling of space-time harmonics.[25,26] For practical finite length structures, the bifurcation analysis yields deep insight into the TL behaviour and underlying physics.

The dynamics of the bifurcation can be investigated by considering small amplitude disturbances to the limit cycle and then linearising the response about the limit cycle. This linearized system is a linear time periodic (LTP or *T-periodic*) SSM; it enables us to find the general solution that describes the time evolution of fluctuations and perturbations $\delta\mathbf{x}(t)$, provided that these $\delta\mathbf{x}$ values remain small compared to the limit cycle state $\bar{\mathbf{x}}(t)$. Traditionally, studies of the linearised response yield insight into the stability of the nonlinear system. Importantly, the predictions made using NLD theory do not rely on restrictive assumptions such as a weak nonlinearity, periodicity or homogenity, and structure size or topology.

In the following, Section II discusses the linearisation of the SSM about the steady state solution (the limit cycle), where the spontaneously generated autonomous frequencies are identified as well as their waveforms. In Section III, the relationship between the autonomous frequencies and the stability of the limit cycle is established. Section IV presents the results and findings when the framework is applied to a varactor-loaded CRLH TL. Such an analytical framework is essential for realising the potential of such structures for signal processing and waveguiding applications at terahertz and optical wavelengths.

II. LINEARIZATION AND FLOQUET THEORY

We consider the application of NLD theory to the NL CRLH TL structure shown in Fig. 1, consisting of a cascade

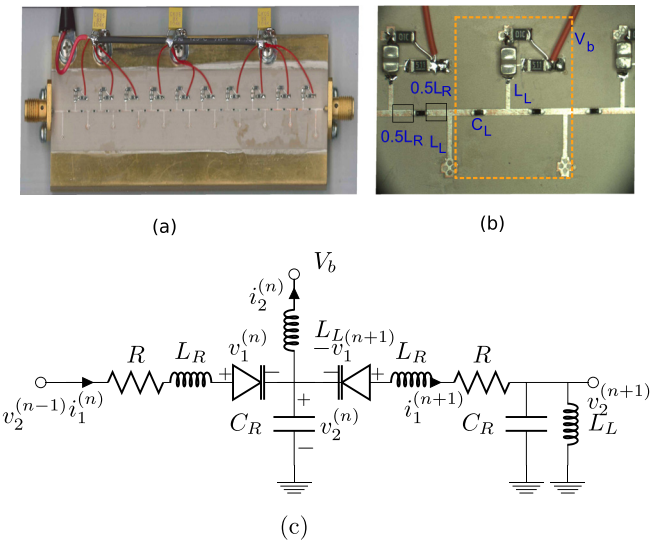

FIG. 1. (a) A 20-stage NL CRLH TL with input (left) and output (right) SMA coaxial connectors. (b) A zoomed view showing the varactors and biasing circuitry. The region inside the highlighted box identifies two unit cells, and the microstrip sections are modelled as inductances and parasitic capacitances (not shown in the figure). (c) Lumped circuit model of two unit cells of an N-stage NL CRLH TL. Nonlinearity is implemented with varactors having voltage dependent capacitance C_L, see (A1). Typical values: $L_L = 1.797$ nH, $C_R = 1.100$ pF, $L_R = 2.700$ nH, and $C_L = 0.730$ pF at bias voltage $V_b = +1.290$ V for a balanced configuration.[27]

of identical unit cells based on series and shunt connected microstrip transmission lines and discrete chip varactor diodes. A lumped element equivalent circuit model (Fig. 1(c)) is available that accurately represents the small signal frequency response and large amplitude nonlinearity.

The inductor currents and capacitor voltages are chosen as the state variables to construct state vector $\mathbf{x}$ in (1), and hence, the dimensionality of the NLD model (length of vector $\mathbf{x}$) equals the number of reactive circuit elements. These states are proportional to the energy storage mechanisms within the structure. In general, state space modelling allows $\mathbf{x}(t)$ to contain any variables that describe the time varying nature of the physical system. For instance, it can be the displacement and the velocity of an elastic medium or the pressure and the velocity of an acoustic wave. Thus, the following analysis can be considered to be applicable to a large class of physical systems.

With a view to applications of these structures, we consider the case of sinusoidal excitation and numerically solve (1) to obtain values for all the states at discrete steps in time. The observation of these solutions shows that the system reaches a limit cycle whenever the input is relatively weak. Physically, this means that the system is stable, whereby fluctuations arising from the background thermal noise do not lead to unbound growth over time of the system states. Increasing the input power renders the limit cycle to be unstable; this means that small fluctuations at certain autonomous frequencies get amplified through a process of energy transfer from the input pump excitation to the autonomous frequency components. The exact values of these autonomous frequencies are determined by the system characteristics, which, unlike linear systems, are functions of the input

level and frequency. Generally speaking, the autonomous and the input frequencies are incommensurate. In this context, the onset at which the input excites autonomous components identifies a bifurcation condition. In this case, the limit cycle *bifurcates* into a quasi-periodic solution (a torus). Such phenomena have been observed experimentally in microwave TLs[12,16] and have been interpreted as parametric behaviour consistent with experience with weak nonlinearities in optical materials.[8]

A. Linearization at the limit cycle

We assume that $\mathbf{x}(t)$ in (1) can be decomposed into two components: the values at the limit cycle $\bar{\mathbf{x}}(t)$ and the perturbation $\delta\mathbf{x}(t)$ about this limit cycle

$$\mathbf{x}(t) = \bar{\mathbf{x}}(t) + \delta\mathbf{x}(t). \tag{2}$$

The state vector $\bar{\mathbf{x}}$ encapsulates the effect of the pump frequency f_P as well as its integer higher harmonics mf_P. The inclusion of higher harmonics can be crucial for accurate performance prediction. In an extreme case, for instance, the presence of higher harmonics on a dispersive-less nonlinear right handed TL plays an essential role in shock wave formation.[28] By substituting (2) into (1), expanding in Taylor's series, and then neglecting higher order terms, an expression for the linearisation of the disturbance about the limit cycle is obtained

$$\delta\dot{\mathbf{x}} = \left.\frac{\partial f}{\partial \mathbf{x}}\right|_{\bar{\mathbf{x}}} \delta\mathbf{x} = \mathbf{J}(\mathbf{x},t)|_{\bar{\mathbf{x}}}\,\delta\mathbf{x}, \tag{3}$$

where $\mathbf{J}$ is the Jacobian evaluated at the limit cycle and is a *T-periodic* function of time. Thus, (3) describes a Linear Time Periodic (LTP) system of differential equations with a minimum period $T = 1/f_P$. Despite the periodicity of $\mathbf{J}(t)$, the solution of (3) is not necessarily periodic in T. The linearization process presented here is not very different from linearizing at an equilibrium point, which is routinely used to investigate the stability of electrical and mechanical systems,[29] whereas for linear time-invariant (LTI) systems, the Jacobian is a constant valued matrix. It is worth noting that linearization is extendable to other more complex limit sets such as toruses and strange attractors.[23] For such complex limit sets, the Jacobian will be defined on complex manifolds and will be neither constant nor periodic.

B. General solution of the LTP system

A general solution of the n-dimension LTP system in (3) describing the time evolution of $\delta\mathbf{x}(t)$ for time $t \geq t_o$ depends on the initial condition of the states $\delta\mathbf{x}(t_o)$ and knowledge of the state transition matrix $\mathbf{\Phi}(t,t_o) = \mathbf{X}(t)\mathbf{X}^{-1}(t_o)$, where $\mathbf{X}(t)$ is a fundamental matrix of the linearised system.[30,31] We then have for any $t \geq t_o$

$$\delta\mathbf{x}(t) = \mathbf{\Phi}(t,t_o)\,\delta\mathbf{x}(t_o). \tag{4}$$

Upon substitution of (4) into (3), we also observe that $\mathbf{\Phi}(t,t_o)$ satisfies the same time periodic expression

$$\dot{\mathbf{\Phi}}(t,t_o) = \mathbf{J}(\mathbf{x},t)|_{\bar{\mathbf{x}}}\,\mathbf{\Phi}(t,t_o), \quad \mathbf{\Phi}(t_o,t_o) = \mathbf{I}. \tag{5}$$

Since matrix $\mathbf{J}$ is T-periodic, Floquet theory can be applied to write[30,31]

$$\mathbf{\Phi}(t,t_o) = \mathbf{P}(t)\,e^{(t-t_o)\mathbf{R}}, \tag{6}$$

where the $n \times n$ matrices $\mathbf{P}$ and $\mathbf{R}$ are defined as[31]

$$e^{\mathbf{R}T} = \mathbf{\Phi}(T+t_o,t_o), \tag{7}$$

$$\mathbf{P}(t) = \mathbf{\Phi}(t,t_o)\,e^{-\mathbf{R}(t-t_o)}; \quad \mathbf{P}(t_o) = \mathbf{I}. \tag{8}$$

Matrix $\mathbf{P}(t)$ is also T-periodic ($\mathbf{P}(t+T) = \mathbf{P}(t)$). The eigenvalues ρ_k $(k = 1,2\ldots n)$ of $\mathbf{\Phi}(T+t_o,t_o)$ in (7) are called the Floquet multipliers and are, in general, either purely real valued or occur as complex conjugate pairs. Note that (6) can be considered as the generalized time domain Bloch-Floquet (BF) condition in periodic structures.

If the eigenvalues of $\mathbf{R}$ are distinct, the matrix $e^{\mathbf{R}T}$ can be diagonalized by the appropriate similarity transformation $e^{\mathbf{R}T} = \mathbf{S}\,e^{\tilde{\mathbf{R}}T}\,\mathbf{S}^{-1}$, where $\tilde{\mathbf{R}}$ is diagonal. Noting that for matrix functions[32] $\mathbf{S}\,e^{\tilde{\mathbf{R}}T}\,\mathbf{S}^{-1} = e^{\mathbf{S}\tilde{\mathbf{R}}T\mathbf{S}^{-1}}$, we then have $\mathbf{R} = \mathbf{S}\,\tilde{\mathbf{R}}\,\mathbf{S}^{-1}$, and hence, $\delta\mathbf{x}(t)$ can be written as

$$\delta\mathbf{x}(t) = \tilde{\mathbf{P}}(t)\,e^{t\tilde{\mathbf{R}}}\,(\mathbf{S}\,e^{t_o\tilde{\mathbf{R}}})^{-1}\,\delta\mathbf{x}(t_o), \tag{9}$$

where $\tilde{\mathbf{P}}(t) = \mathbf{P}(t)\mathbf{S}$. Since matrices $e^{\mathbf{R}T}$ and $e^{\tilde{\mathbf{R}}T}$ are similar, they share the same eigenvalues $\rho_k = |\rho_k|\exp(i\theta_k)$. Furthermore, the diagonal elements of the diagonal matrix $e^{\tilde{\mathbf{R}}T}$ are these eigenvalues, which we write as $\rho_k = e^{\mu_k T}$, where $\mu_k \equiv \sigma_k + i\theta_k/T$ are the Floquet exponents $(\sigma_k = \ln|\rho_k|/T)$. Since $(\mathbf{S}\,e^{t_o\tilde{\mathbf{R}}})^{-1}\delta\mathbf{x}(t_o)$ is a constant, $\mathbf{Y}(t) \equiv \tilde{\mathbf{P}}(t)e^{t\tilde{\mathbf{R}}}$ is also a fundamental matrix of the linearised system. By the definition of fundamental matrices, the columns $\mathbf{y}_k(t)$ of $\mathbf{Y}(t)$ are independent solutions of (3).[30] The k^{th} independent solution can be written as

$$\mathbf{y}_k(t) = e^{\mu_k t}\tilde{\mathbf{p}}_k(t), \tag{10}$$

where $\tilde{\mathbf{p}}_k(t)$ is the k^{th} column of $\tilde{\mathbf{P}}(t)$. In the following, it will be useful to evaluate the real-valued observable system response. This can be achieved by the proper combination of $\mathbf{y}_k(t)$ and its associated complex conjugate solution. One set of solutions is

$$\mathbf{y}_k(t) = 2\,e^{\sigma_k t}\left[\Re(\tilde{\mathbf{p}}_k(t))\cos(\theta_k t/T) - \Im(\tilde{\mathbf{p}}_k(t))\sin(\theta_k t/T)\right] \tag{11}$$

which is equivalent to the real part of $\mathbf{y}_k(t)$ in (10). Similarly, an independent set of real solutions is readily obtained from the imaginary part of $\mathbf{y}_k(t)$.

The expression (11) explicitly shows that for $|\sigma_k \approx 0|$ or $|\rho_k \approx 1|$, $\mathbf{y}_k(t)$ is the product of two time harmonic terms, T-period $\tilde{\mathbf{p}}_k(t)$, and the other at an unrelated frequency determined by the phase angle of the Floquet multiplier, θ_k/T. Since the solutions of linear time varying differential equations form a vector space, the observed solution is the linear combination of $\mathbf{y}_k(t)$

$$\mathbf{y}(t) = \sum_{k=1}^{n} c_k\,\mathbf{y}_k(t), \tag{12}$$

where c_k are the constants and n is the dimension of the state vector. The set of independent solutions $\mathbf{y}_k(t)$ forms the basis of the space of solutions to (3). Note that although the evaluation of $\delta\mathbf{x}(t)$ from (4) will reveal the behaviour of the system to any initial conditions $\delta\mathbf{x}(t_o)$, the evaluation of (10) or (12) reveals the same characteristic system behaviour in the $\mathbf{y}_k(t)$ solutions, independent of any initial condition considerations. In the following, we use (10) as a predictor for $\mathbf{y}_k(t)$, having the same characteristic behaviour as disturbances $\delta\mathbf{x}(t)$ to the limit cycle $\bar{\mathbf{x}}(t)$.

III. BIFURCATION OF AUTONOMOUS FREQUENCIES

A consequence of complex valued Floquet multipliers is the generation of autonomous frequencies in the solution to (3). From (10), the value of the k^{th} solution at time $t+T$ is given by

$$\mathbf{y}_k(t+T) = \rho_k\,\mathbf{y}_k(t) = e^{\mu_k T}\mathbf{y}_k(t). \tag{13}$$

As with ρ_k, μ_k can be complex and is a function of the system characteristics, input excitation amplitude, and frequency. If the magnitude of the k^{th} Floquet multiplier $|\rho_k|$ is slightly greater than one, i.e., the multiplier crosses the unit circle in the complex plane, then $\mathbf{y}(t)$ increases in amplitude with time, as does $\delta\mathbf{x}(t)$, indicating the onset of instability that can result from a change in the operating conditions. For the case where only one or a few Floquet multipliers have magnitudes just greater than unity, the response $\mathbf{y}(t)$ will be dominated by the $e^{\mu_k t}$ terms associated with this/these multipliers.

While too large an increase in the magnitude of the disturbance $\delta\mathbf{x}$ violates the linearisation assumptions (i.e., higher order terms in the Taylor series expansion that led to (3) need to be considered), experimental observations have shown that it is possible for the disturbances to remain relatively small, which can be interpreted as the transformation of the limit cycle into a torus through the generation of autonomous frequencies related to the complex valued Floquet multipliers $\rho_k = |\rho_k|\exp(i\theta_k)$, where from (11), the values of these frequencies are given by

$$f_m^{(k)} = f_P\left|\frac{\theta_k}{2\pi} + m\right|, \tag{14}$$

where the superscript k emphasizes that the frequency is associated with the multiplier ρ_k. The phase ambiguity of $2m\pi$, $m = 0, \pm1, \pm2, \ldots$ suggests an infinite number of autonomous frequencies. For example, $f_0^{(k)} = |\theta_k/2\pi|f_P$ and $f_{-1}^{(k)} = f_P - f_0^{(k)}$. The generation of potentially an infinite number of autonomous frequencies is due to the coupling of the time harmonics, resulting from the periodicity of $\tilde{\mathbf{p}}_k(t)$, which is the time domain equivalent of spatial harmonics in *spatial* periodic structures. If the largest Floquet multiplier is purely real valued, then the unit circle crossing corresponds to a flip-type bifurcation,[23] leading to the observation of bistability or multistability.[17] Complex valued Floquet multipliers occur as conjugate pairs, leading to Hopf-type bifurcations[23] and observation of autonomous frequency generation. The Floquet analysis provides a valuable tool that links the generation of the autonomous frequencies to the position of the corresponding Floquet multipliers relative to the unit circle in the complex plane.

From (10) and (11), it is clear that the frequency content of $\mathbf{y}_k(t)$ consists of frequencies

$$\omega = |\omega_k \pm m\omega_p|, \quad m = 1, 2, \ldots. \tag{15}$$

Note that (15) automatically calculates the sum and difference frequencies traditionally associated with nonlinear mixing products.

It is worth emphasizing that the stability analysis carried out here shows that for each ρ_k crossing the unit circle, an infinite number of autonomous frequencies are generated. This is to be compared to three wave mixing where interactions are limited to three waves only (pump, signal, and idler). For band limited structures, such as CRLH TLs, higher frequency components are attenuated, thereby restricting the number of waves that can be observed in practice.

For an infinitely long TL, the spatial regularity will augment the temporal Bloch-Floquet (BF) condition shown by (6) with an extra spatial BF condition, resulting in a dispersion relation between the spatial and temporal characteristic multipliers. Equivalently, spatial characteristic multipliers, β_k, are nothing but the complex wave number. Hence, the propagation can be described using the space time harmonics. In general, both β_k and μ_k can be complex. When μ is imaginary, an imaginary value of β corresponds to an allowed propagation mode, while a real β indicates a stop band. The distinction between the temporal (complex frequency) and spatial (complex propagation constant) was previously investigated in the context of a spatio-temporal varying right handed TL.[25,33]

IV. RESULTS AND DISCUSSION

The framework presented in Sections II and III is applied here to a lumped circuit model for the 20-stage transmission line shown in Fig. 1 to determine the spontaneously generated autonomous frequencies and their waveforms. There are 82 state variables, and hence, $\mathbf{x}$ is an $n = 82$-length vector. The SSM in (1) was obtained by applying basic circuit theory to construct an analytical formulation for the function f and the Jacobian $\mathbf{J}(\mathbf{x}, t)$ in the linearized form (3). The voltage and currents shown in Fig. 1(c) were relabelled to form the elements of $\mathbf{x}$. For the sake of completeness, the nonlinear and linearized state space equations are presented in the Appendix section. The nodal equations of the very first and last cells are slightly modified to maintain a symmetric CRLH structure[4] due to the connection with the source and the load, respectively. In the absence of the pump power, the system is a linear time invariant (LTI) and the varactor series capacitances are determined by the bias voltage as given by (A10). By assuming that the LTI TL is infinitely long, the dispersion relation of the linear time invariant TL can be obtained analytically via the relation[4]

$$\kappa^2 = 4\sin^2\left(\frac{\beta p}{2}\right), \tag{16}$$

where $\kappa = \sqrt{-Z_{se}Y_{sh}}$, and $Z_{se} = i(\omega L_R - 1/\omega C_{L0})$ and $Y_{sh} = i(\omega C_R - 1/\omega L_L)$ are the series impedance and shunt admittance, respectively. In (16), βp is the phase shift per unit cell at a given angular frequency ω, where p is the physical length of the unit cell.[4] Fig. 2 shows the dispersion relation given by (16). The plot highlights regions where backward waves (the phase and group velocities v_{ph} and v_g) have opposite directions.

For the 20-stage NL CRLH TL shown in Fig. 1, the source excitation consisted of a single sinewave (pump) excitation connected to the input of the first unit cell, with pump frequency f_P and voltage amplitude V_P. This sinusoidal source contributed to one element of the $n = 82$ length $\mathbf{u}(t)$ vector, with other 20 of the $\mathbf{u}(t)$ elements corresponding to the constant valued varactor bias voltage V_b for each of the 20 unit cells (Fig. 1). Then, numerical values for the states $\mathbf{x}(t)$ over a range of discrete time steps were obtained by numerically solving this system of first order differential equations (implemented using Matlab's *ode45* solver[34]), for a sinusoidal excitation at the input of the structure. By allowing the solution to run for a sufficiently long time (from time $t = 0$ to $t = t_o \approx 2 - 4\,\mu s$), the steady state limit cycle $\bar{\mathbf{x}}(t)$ was established.[35] The state transition matrix $\mathbf{\Phi}(t, t_o)$ was then calculated by solving (5) from time $t = t_o$ to $t = t_o + T$ using the *ode45* solver. We note that Jacobian's time varying term associated state variable varactor voltages $\mathbf{x}_{4n}$ in (A1) are re-evaluated at each time step using the limit cycle values $\bar{\mathbf{x}}(t)$.

The Floquet multipliers are computed by evaluating the eigenvalues of $\Phi(t_o + T, t_o)$, with the corresponding frequencies determined from (14). The pump level V_P is increased, and the above calculations are repeated until one (or more) multiplier(s) just cross(es) the unit circle ($|\rho_k| \approx 1$ at $V_P = V_{P0}$); this is the onset of bifurcation and identifies the generation of the autonomous frequencies. Fig. 3 shows the calculated frequencies ($f_0^{(1)}$ only) using both (14) and frequencies identified in the Fourier transform of waveforms $\mathbf{x}(t)$ that are solutions to (1) for $t \geq t_o$. It is clear that the stability analysis accurately predicts the values of the autonomous frequencies. Additionally, there is a good agreement between the behaviour of the calculated V_{P0} (Fig. 3(b)) and the measurement[27] of the structure in Fig. 1 (Fig. 3(c)). However, there is some discrepancy above 5 GHz, which is attributed to the parasitic effects, not taken into account in the state space model.[19] These parasitic effects introduce a dip (absorption) in the LTI transmission coefficient at around 2 GHz that changes the system dynamics. Nevertheless, the non-restrictive nature of the state space formalism permits the application of more sophisticated models and the bifurcation analysis will not change.

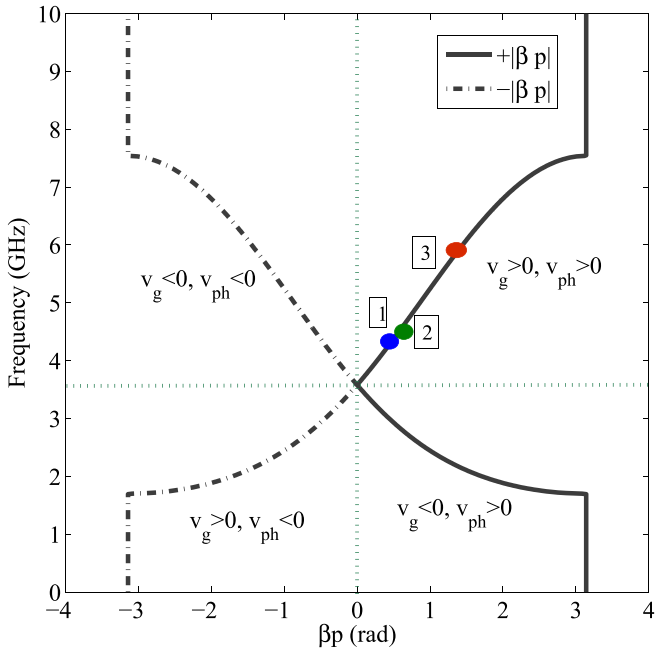

FIG. 2. The dispersion relation of the linear time invariant TL. The dots 1, 2, and 3 represent the loci of the pump frequencies $f_P = 4.400$ GHz, $f_P = 4.500$ GHz, and $f_P = 5.800$ GHz, respectively.

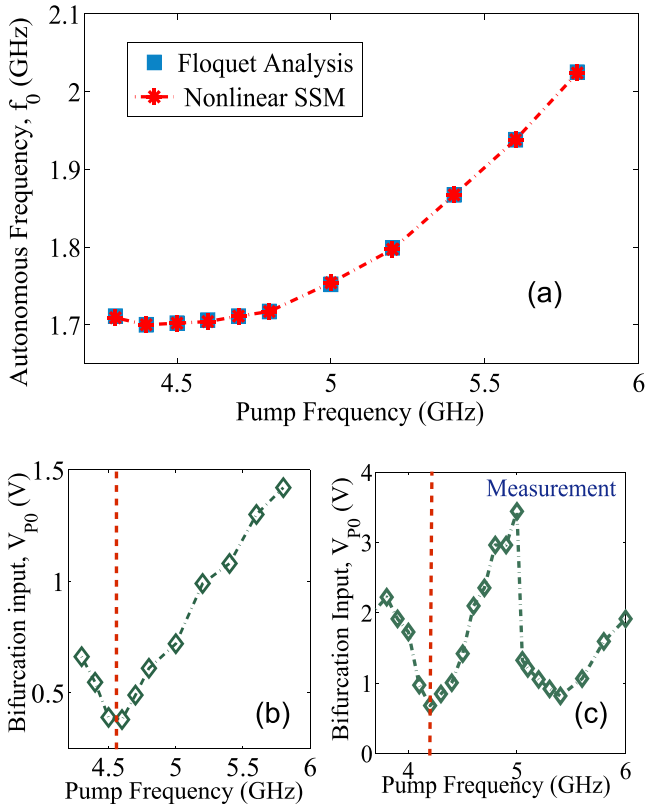

FIG. 3. (a) The $f_0^{(1)}$ values calculated over $f_P = 4.300$ to 5.800 GHz. (b) The calculated onset of bifurcation, V_{P0}. (c) The measured[27] V_{P0} versus f_P.

Fig. 3(b) shows that the onset of bifurcation voltage, V_{P0}, attains its minimum in the vicinity of the 4.400 GHz–4.500 GHz interval, suggesting a change in the bifurcation nature. In fact, it will be shown in Sections IV A and IV B that at the onset of bifurcation, only one Floquet multiplier crosses the unit circle when $f_P = 4.500$ GHz, which corresponds to one set of autonomous frequencies $f_m^{(1)}$. However, when f_P is slightly decreased to 4.400 GHz, two sets of incommensurate autonomous frequencies $f_m^{(1)}$ and $f_m^{(2)}$ emerge. Equivalently, this means that two Floquet multipliers simultaneously cross the unit circle.

A. One dominant multiplier

Figure 4(a) depicts the loci of the three most dominant multipliers as a function of the pump voltage for a pump

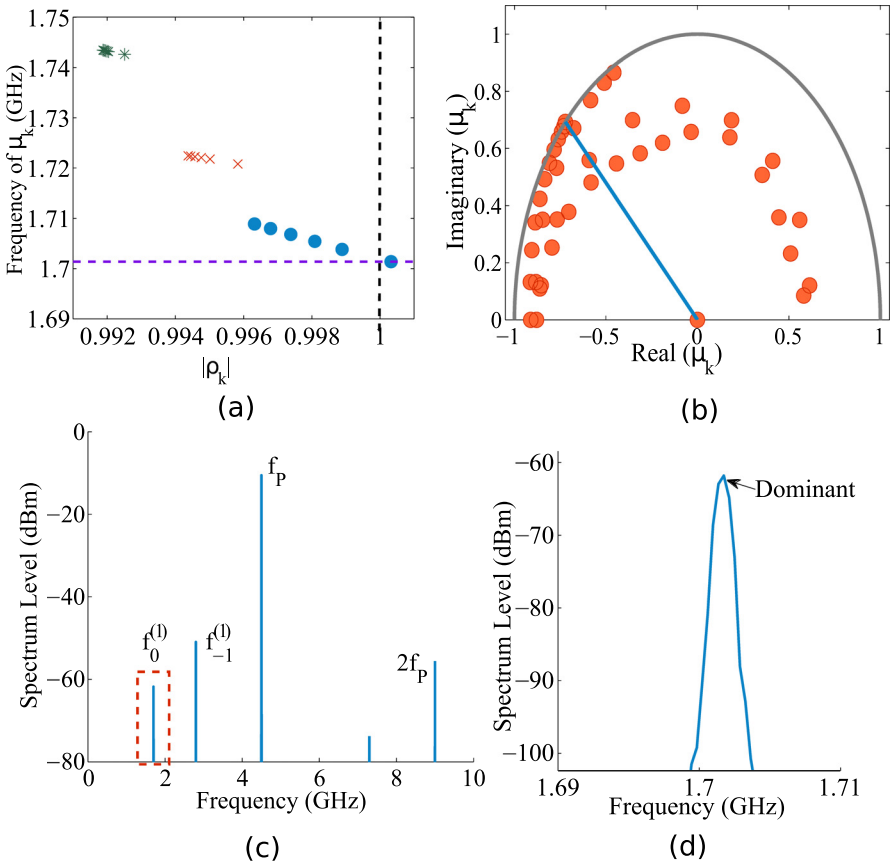

FIG. 4. One autonomous frequency at $f_0^{(1)} = 1.701$ GHz: $f_P = 4.500$ GHz. (a) The loci of the magnitude of the three multipliers which have the largest magnitude, calculated as a function of the pump voltage V_P. V_P takes the values of 0.14, 0.190, 0.240, 0.290, 0.340, and 0.390 V, where $V_{P0} = 0.390$ V. (b) Multipliers located in the complex plane together with the unit circle. Since multipliers appear as complex pairs, only half the circle is shown. (c) The Fourier spectrum of the output voltage obtained by solving (1) for $V_P = V_{P0}$. (d) Zoomed view of the spectrum.

frequency $f_P = 4.5$ GHz until bifurcation occurs. As depicted in Fig. 4, the autonomous frequencies depend on the pump voltage V_P. This is expected since as V_P changes, the limit cycle size changes as well, which alters the linearized system (3). When f_P is 4.500 GHz, only one multiplier crosses the unit circle (vertical dashed line in Fig. 4(a)). The Fourier spectrum of the output voltage confirms this by showing only one frequency component $f_0^{(1)} = 1.701$ GHz corresponding to the dominant multiplier (Figs. 4(b) and 4(c)). The mixing product $f_{-1}^{(1)} = |f_0^{(1)} - f_P|$ also appears.

B. Two dominant multipliers

Repeating the analysis in Section IV A, but when f_P is slightly decreased to 4.400 GHz (Fig. 5(a)), two multipliers cross the unit circle. Examining the Fourier spectrum (Figs. 5(b) and 5(c)), it is clear that both the multipliers have an effect on the spectral content. The two independent solutions $\mathbf{y}_1(t)$ and $\mathbf{y}_2(t)$, corresponding to the two dominant multipliers, evolve independently in the solution space.

The versatility in determining $\mathbf{x}(t)$ at any time through the solution of (1) means that we can observe both the temporal and spatial behaviour of all the state variables in the structure. As an example, Fig. 6 shows the distributions of the spectral amplitudes at frequencies $f_0^{(1)}, f_0^{(2)}$, and $f_{-1}^{(1)}, f_{-1}^{(2)}$, where $f_m^{(1)}$ and $f_m^{(2)}$ correspond to the first maximum and second maximum $|\rho_k|$ values, calculated from those components of vector $\mathbf{x}(t)$ corresponding to the voltages across the shunt capacitances C_R in each stage, for $f_p = 4.400$ GHz and $V_P = 0.547$ V. Also shown are the spectral amplitudes calculated from the two time series $\mathbf{y}_1(t)$ and $\mathbf{y}_2(t)$ in (11). Very good agreement between the two can be observed, further illustrating the utility and the accuracy of the stability analysis. It is also worth noting that although the $f_0^{(1)}$ and $f_0^{(2)}$ of both the multipliers are very close in value (1.698 and 1.711 GHz), their spatial amplitude profiles are quite different. These two frequencies are close to the lowest Bragg frequency ($f_c \approx 1.7$ GHz, refer to Fig. 2) where the TL can be considered to act like a photonic crystal. Furthermore, the amplitude variation of the $f_{-1}^{(k)}$ terms (2.702 and 2.689 GHz) suggests a transfer of power from the 4.400 GHz pump to the backward propagating $f_{-1}^{(k)}$ components, consistent with the three wave mixing explanation (parametric amplification). This can be better understood by referring to Fig. 7 which plots the relative phase and normalized power of the $f_{-1}^{(1)} = 1.698$GHz and $f_0^{(1)} = 2.702$ GHz components of the C_R capacitor voltages at the output of each unit cell. The $f_{-1}^{(1)}$ frequency value is equal to the Bragg frequency, and hence, the slope of the phase is $\pm\pi$. The two autonomous components are in the left hand region (Fig. 2), implying that the phase and group velocities are opposite. The phase velocity is pointing toward the load whenever the slope of the phase is negative. According to the sign convention of the state variables shown in Fig. 1(c), positive power means that energy is transferred toward the load. From Fig. 7, it is found that the directions of the phase velocity (proportional to the slope of the phase) and the group velocity (parallel to the direction of power flow) are always opposite, a characteristic of backward waves. For the first ten stages, power is *pumped* from the strong 4.400 GHz wave to the two autonomous components, as they propagate

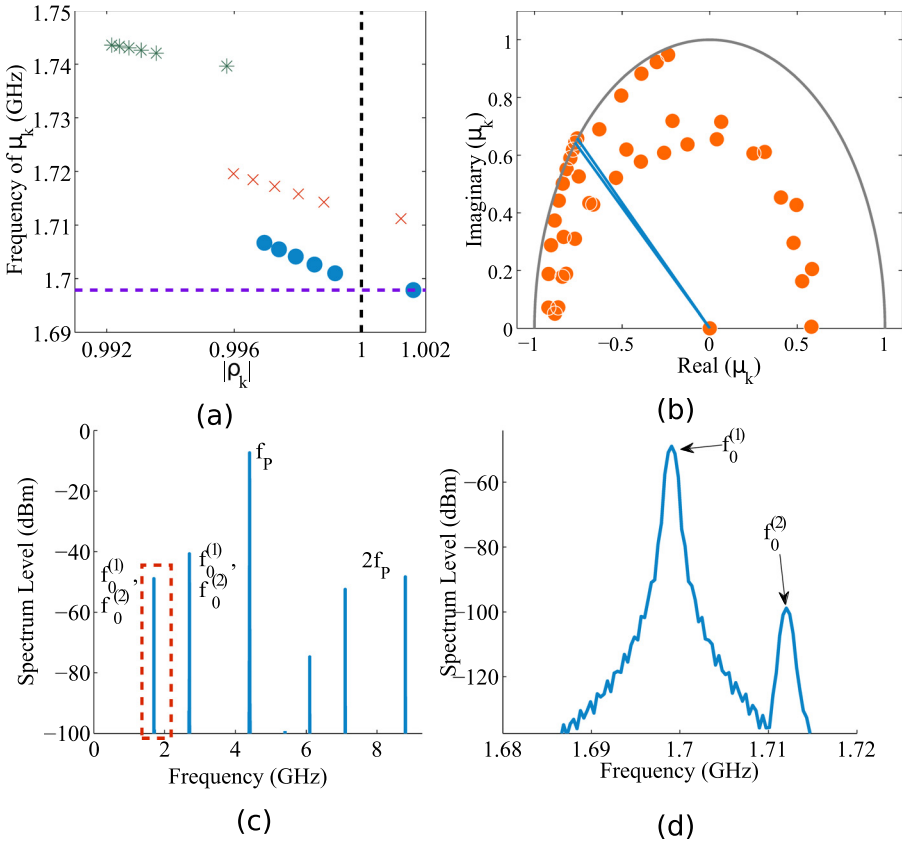

FIG. 5. Two autonomous frequencies at $f_0^{(1)} = 1.698$ GHz and $f_0^{(2)} = 1.711$ GHz: as for Fig. 4 but for $f_P = 4.400$ GHz. V_P takes the values of 0.300, 0.350, 0.400, 0.450, 0.500, and 0.547 V, where $V_{P0} = 0.547$ V. Two closely spaced autonomous frequencies are observed.

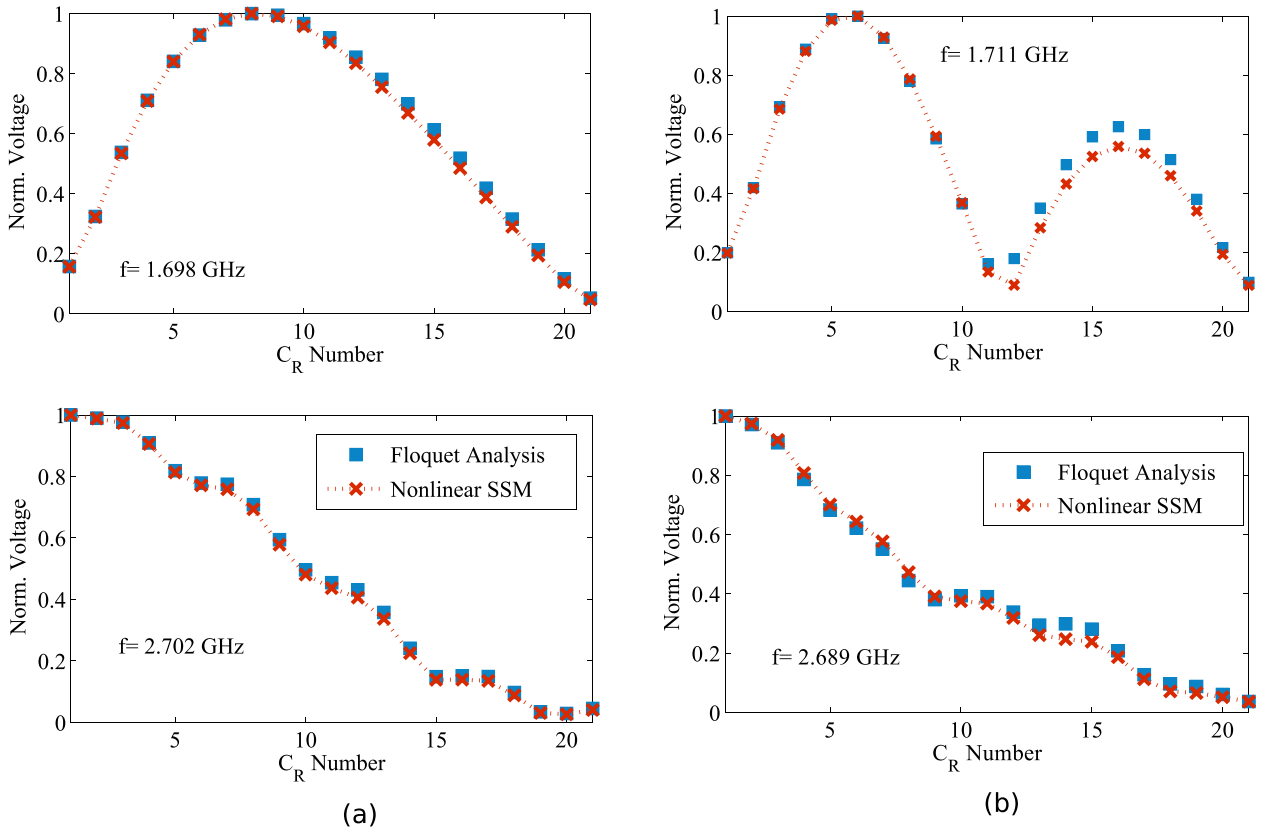

FIG. 6. The normalised waveform distribution of the voltage across the shunt capacitance C_R along the NL CRLH TL, when $f_P = 4.4$ GHz. (a) The most dominant multiplier. (b) The second dominant multiplier.

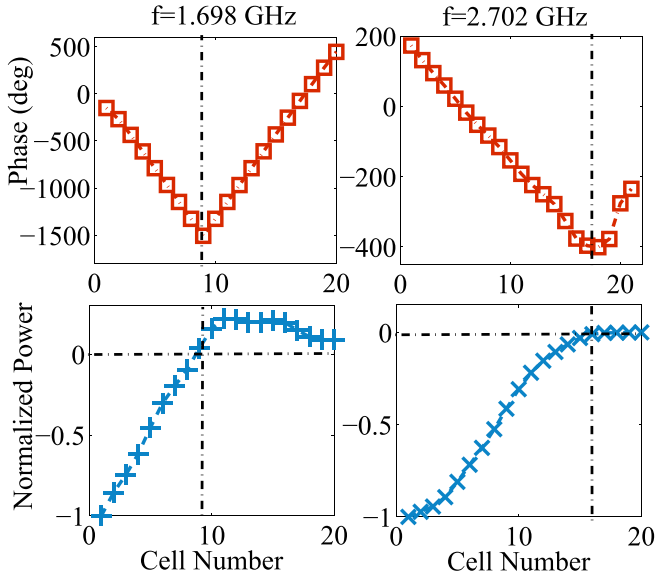

FIG. 7. Top: Calculated Phase and Bottom: Normalized Power of the autonomous components when $f_P = 4.400$ GHz.

toward the source, indicating a parametric process involving three waves, where their frequencies are related by (14).

Additionally, the pumped frequency is raised to $f_P = 5.800$ GHz (Fig. 8). In this case, one of the autonomous frequencies is in the right hand region (above the band edge $1/2\pi\sqrt{L_R C_L} \approx 3.58$ GHz, refer to Fig. 1). Again, the stability analysis can predict the waveforms of the autonomous frequencies accurately. Interestingly, the amplitude of the waveform at frequency $f = 2.024$ GHz is not smooth, suggesting that the interaction is atomic and cannot be described using the effective medium theory.

It is worth noting that the Floquet analysis provides insight into how the autonomous frequencies and their

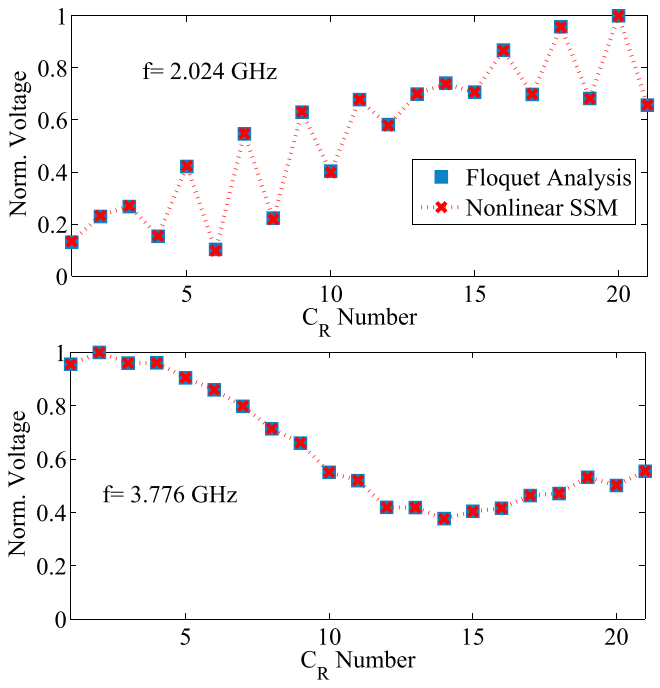

FIG. 8. The normalised line voltage distribution of the autonomous frequencies along the NL CRLH TL, when $f_P = 5.8$ GHz and $V_{P0} = 1.4$ V.

waveforms are related to the system parameters via the *T-Periodic* Jacobian matrix. Although a brute force nonlinear solver can predict the values of the frequencies and their waveforms, it does not explain why the autonomous frequencies attain certain values and how they depend on the system parameters and input power and frequency. However, the brute force nonlinear solver was indeed invoked to validate the predictions of Floquet analysis.

The onset of bifurcation can be understood by considering the condition at which the generation of a Stokes wave becomes possible in a Stimulated Brillouin Scattering (SBS) process.[8] For an optical medium, an intense pump of frequency f_P causes electrostriction, resulting in a generation of an acoustic wave of frequency f_1. Although it has a small amplitude, the acoustic wave beats with the pump to reinforce a Stokes wave (at frequency $f_1 = f_P - f_2$), generated via the thermal fluctuations. This wave in turn beats with the pump to reinforce the acoustic wave further. The positive feedback behaviour of the two interactions results in an exponential growth of the amplitude of the Stokes wave. In the CRLH case, the pump beats with the thermally excited autonomous components. As a result, the amplitudes of the autonomous components get amplified.

As in SBS, the positive feedback process is only possible when the input pump level exceeds a threshold, which is the onset of bifurcation.[8]

V. CONCLUSION

In this article, we applied the rigorous NLD theory to study the stability of a NL CRLH TL structure. NLD theory allows the decomposition of the wave behaviour into a spatially distributed array of time varying states (voltages and currents) that display limit cycle behaviour that is periodic with the pump excitation. For excitation levels above a threshold, additional autonomous frequency components are generated, which can be observed to wind around the limit cycle forming a dense torus. The autonomous frequencies depend on the system parameters and the input excitation. When the pump level is over a certain threshold, the limit cycle bifurcates into a torus and the autonomous components are sustained. The NLD approach takes into account the possible interactions via the higher harmonics; it is general in terms of the nature and the strength of nonlinearity; it is not limited by the effective media approximation. While the approach taken here does not predict the steady state amplitudes of the autonomous frequencies (a consequence of neglecting higher order terms with the linearisation of (3)), it does accurately predict the waveform, the values of the autonomous frequencies, the pump power threshold where these appear, and synthesis of the system response for selected autonomous frequency components and provides a convenient mechanism to track individual autonomous frequency components throughout the structure. This approach provides an important investigative tool for characterising NL CRLH TL structures, with a view to aid the design process and realise potential applications for these structures.

Moreover, the Floquet analysis is a time domain method which emerges directly from the linearization of the state

space model; this is contrasted to wave mixing and Harmonic Balance (HB) methods which are formulated in the frequency domain. Additionally, the autonomous frequencies are obtained from the characteristic (Floquet) multipliers which are determined by the system parameters (encapsulated in the time periodic Jacobian). On the other hand, HB techniques will usually assume a range or set of possible frequencies and solve the circuit for each one to determine the system poles (for example, $Z(f)$ as in Ref. 27); it does not provide deep insight into why the autonomous frequencies take certain values.

APPENDIX: STATE SPACE MODEL

The series and shunt connected microstrip sections are modelled by inductors L_R, L_L, and C_R. The inductor currents and capacitor voltages are the state variables and labelled as shown in Fig. 9. The capacitors C_L model the reverse-biased varactor diode's depletion capacitance, which is related to the voltage x_{4n}, $n = 1, 2, \ldots, N$ across the n^{th} diode by[36]

$$C_L = \frac{C_{j0}}{\left(1 + (-1)^n x_{4n}/\psi_0\right)^{\gamma}}, \tag{A1}$$

where C_{j0}, ψ_0, and γ were experimentally found to be 1.200pF, 2.055 V, and 1.000, respectively. The $(-1)^n$ factor is due to the back to back connection of the varactors (Fig. 1). The state space equations can be formulated for the circuit model in Fig. 1(c) as

$$\dot{x}_{4n-1} = \frac{1}{L_R}\left(x_{4n-2} - R x_{4n-1} - x_{4n} - x_{4n+2}\right), \tag{A2}$$

$$\dot{x}_{4n+1} = \frac{1}{L_L}\left(x_{4n+2} - V_b\right), \tag{A3}$$

$$\dot{x}_{4n+2} = \frac{1}{C_R}\left(x_{4n-1} - x_{4n+1} - x_{4n+3}\right), \tag{A4}$$

$$\dot{x}_{4n+5} = \frac{1}{L_L} x_{4n+6}, \tag{A5}$$

$$\dot{x}_{4n+6} = \frac{1}{C_R}\left(x_{4n+3} - x_{4n+5} - x_{4n+7}\right) \tag{A6}$$

and

$$\dot{x}_{4n} = \frac{1}{C_L(x_{4n})} x_{4n-1}. \tag{A7}$$

An equation for x_{4n+3} can be obtained from (A7) by replacing n by $n+4$. All state space equations (A3)–(A6) are linear in the state variables. Hence, the corresponding Jacobian $\mathbf{J}(\mathbf{x}, t)$ elements are just the coefficients of the state variables. The nonlinearity, due to the nonlinear characteristics of the varactors, appears in (A7). It is worth noting that the state space equations are slightly modified for the first and last unit cells, partly due to the presence of the shunt inductor $2L_L$, capacitance $C_R/2$, and the connection to the input source and load, respectively. The linearized form of (A7) is obtained by taking the partial derivative of the right hand side with respect to x_{4n} and x_{4n-1} at the limit cycle solution $\bar{x}_{4n}$ and $\bar{x}_{4n-1}$ to give

$$\delta\dot{x}_{4n} = \frac{1}{C_L(\bar{x}_{4n})}\delta x_{4n-1} - \frac{1}{C_L^2(\bar{4}_{4n})}\left[\frac{\partial C_L}{\partial x_{4n}}\right]_{\bar{x}_{4n}} \bar{x}_{4n-1} \cdot \delta x_{4n}. \tag{A8}$$

The coefficients of (A8), which are the Jacobian elements linking δx_{4n-1} and $t\delta x_{4n}$ with $\delta\dot{x}_{4n}$, are *T-periodic* with a minimum period of $T = 1/f_P$. In the absence of the pump, (A6) becomes

$$\delta\dot{x}_{4n} = \frac{1}{C_{L0}}\delta x_{4n-1}, \tag{A9}$$

where

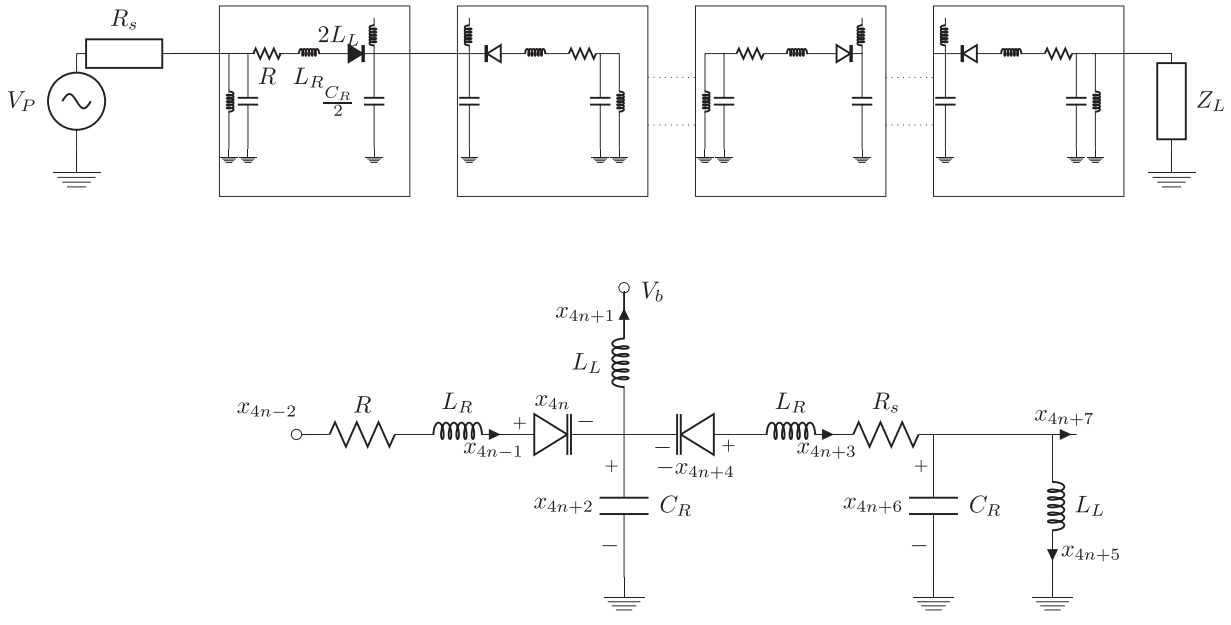

FIG. 9. (Top) The Transmission Line Topology. The source and load impedances are 50 Ω. (Bottom) Two unit cells, where shunt elements are combined together.

$$C_{L0} = \frac{C_{j0}}{\left(1 + \frac{V_b}{\psi_0}\right)^{\gamma}}, \tag{A10}$$

which is constant for a given bias V_b.

[1]V. G. Veselago, Sov. Phys. Usp. **10**, 509 (1968).
[2]J. B. Pendry, Phys. Rev. Lett. **85**, 3966 (2000).
[3]G. V. Eleftheriades and K. G. Balmain, *Negative-Refraction Metamaterials: Fundamental Principles and Applications* (Wiley, Hoboken, 2005).
[4]C. Caloz and T. Itoh, *Electromagnetic Metamaterials: Transmission Line Theory and Microwave Applications* (Wiley, Hoboken, 2005).
[5]C. Caloz, A. Sanada, and T. Itoh, IEEE Trans. Microwave Theory Tech. **52**, 980 (2004).
[6]S. Lim, C. Caloz, and T. Itoh, IEEE Trans. Microwave Theory Tech. **53**, 161 (2005).
[7]A. Grbic and G. V. Eleftheriades, Phys. Rev. Lett. **92**, 117403 (2004).
[8]R. W. Boyd, *Nonlinear Optics*, 3rd ed. (Academic Press, Boston, 2008), includes bibliographical references and index.
[9]M. Lapine, M. Gorkunov, and K. H. Ringhofer, Phys. Rev. E **67**, 065601 (2003).
[10]A. A. Zharov, I. V. Shadrivov, and Y. S. Kivshar, Phys. Rev. Lett. **91**, 037401 (2003).
[11]V. M. Agranovich, Y. R. Shen, R. H. Baughman, and A. A. Zakhidov, Phys. Rev. B **69**, 165112 (2004).
[12]M. Lapine, I. V. Shadrivov, and Y. S. Kivshar, Rev. Mod. Phys. **86**, 1093 (2014).
[13]A. Popov and V. Shalaev, Appl. Phys. B **84**, 131 (2006).
[14]A. B. Kozyrev, H. Kim, and D. W. van der Weide, Appl. Phys. Lett. **88**, 264101 (2006).
[15]A. Kozyrev and D. Van Der Weide, IEEE Trans. Microwave Theory Tech. **53**, 238 (2005).
[16]A. B. Kozyrev and D. W. van der Weide, J. Phys. D: Appl. Phys. **41**, 173001 (2008).
[17]D. A. Powell, I. V. Shadrivov, and Y. S. Kivshar, Appl. Phys. Lett. **92**, 264104 (2008).
[18]L. Chen and G. Milford, in *Proceedings of the Antennas and Propagation Society International Symposium (APSURSI)* (IEEE, 2012), pp. 1–2.
[19]S. Y. Elnaggar and G. N. Milford, in *Proceedings of the International Symposium on Antennas and Propagation (ISAP)* (Hobart, Australia, 2015).
[20]S. Y. Elnaggar and G. N. Milford, in *Proceedings of the 2nd Australian Microwave Symposium (AMS)* (Adelaide, Australia, 2016).
[21]S. H. Strogatz, *Nonlinear Dynamics and Chaos: With Applications to Physics, Biology, Chemistry, and Engineering* (Westview Press, 2014).
[22]H. H. Khalil, *Nonlinear Systems* (Pearson Hall, 2002).
[23]A. Suárez and R. Quéré, *Stability Analysis of Nonlinear Microwave Circuits* (Artech House, 2002).
[24]S. Y. Elnaggar and G. N. Milford, in *Proceedings of the IEEE International Symposium on Antennas and Propagation/USNC-URSI* (Fajardo, Puerto Rico, 2016).
[25]E. S. Cassedy and A. A. Oliner, Proc. IEEE **51**, 1342 (1963).
[26]Y. Hadad, J. C. Soric, and A. Alu, Proc. Natl. Acad. Sci. **113**, 3471–3475 (2016).
[27]M. J. Gibbons and G. N. Milford, in Proceedings of the IEEE MTT-S International Microwave Symposium Digest (MTT) (2011), pp. 1–4.
[28]R. Landauer, J. Appl. Phys. **31**, 479 (1960).
[29]K. Ogata and Y. Yang, *Modern Control Engineering* (Prentice-Hall, Englewood Cliffs, 1970).
[30]R. K. Miller and A. N. Michel, *Ordinary Differential Equations* (Academic Press, 1982).
[31]W. J. Rugh, *Linear System Theory* (Prentice Hall, 1993).
[32]N. J. Higham, *Functions of Matrices: Theory and Computation* (SIAM, 2008).
[33]E. S. Cassedy, Proc. IEEE **55**, 1154 (1967).
[34]MATLAB® Release 2012b (The MathWorks, Inc., Natick, MA, USA).
[35]T. S. Parker and L. Chua, *Practical Numerical Algorithms for Chaotic Systems* (Springer-Verlag, 1989).
[36]A. S. Sedra and K. C. Smith, *Microelectronic Circuits* (Oxford University Press, New York, 1998), Vol. 1.